- 1 Thermal characteristics of permafrost in the steep alpine rock
- 2 walls of the Aiguille du Midi (Mont Blanc Massif, 3842 m a.s.l)

- 4 F. Magnin<sup>1</sup>, P. Deline<sup>1</sup>, L. Ravanel<sup>1</sup>, J. Noetzli<sup>2</sup>, P. Pogliotti<sup>3</sup>
- 5 [1]{EDYTEM Lab, Université de Savoie, CNRS, Le Bourget-du-Lac, France}
- 6 [2]{Glaciology and Geomorphodynamics Group, Department of Geography, University of
- 7 Zurich, Zurich, Switzerland}
- 8 [3]{ARPA Valle d'Aosta, Saint-Christophe, Italy}

- 10 Correspondence to:
- 11 F. Magnin (<u>florence.magnin@univ-savoie.fr</u>)
- 12 P. Deline (<a href="mailto:philip.deline@univ-savoie.fr">philip.deline@univ-savoie.fr</a>)
- 13 L. Ravanel (ludovic.ravanel@univ-savoie.fr)
- J. Noetzli (jeannette.noetzli@geo.uzh.ch)
- P. Pogliotti (paolo.pogliotti@gmail.com)

# **Abstract**

16

17

18

19

20

21

22

23

24

25

26

27

28

29

30

31

32

33

34

35

36

Permafrost and related thermo-hydro-mechanical processes are regarded as probable factors in high alpine rock wall stability, but a lack of field measurements means that the characteristics and processes of rock wall permafrost are poorly understood. To help remedy this situation, in 2005 work began to install a monitoring system at the Aiguille du Midi (3842 m a.s.l). This paper presents temperature records from nine surface sensors (eight years of records) and three 10-m-deep boreholes (four years of records), installed at locations with different surface and bedrock characteristics. Analysis of the temperature data confirm previous studies, some of them being demonstrated empirically for the first time: micrometeorology controls the surface temperature, active layer thicknesses are directly related to aspect and ranged from <2 m to nearly 6 m, warm and cold permafrost (about -1.5°C to -4.5°C at 10-m-depth) coexists within the Aiguille du Midi, resulting in high lateral heat fluxes, thin accumulations of snow and open fractures are cooling factors. Some observations extent existing knowledge: thick snow accumulations warm north faces but cool south faces, possibly inhibit active layer refreezing in winter and delay its thawing in summer. Latent heat consumption due to interstitial water phase changes in bedrock discontinuities possibly dampens the active layer and permafrost changes, whereas an open fractures act as a thermal cutoff in the sub-surface thermal regime. Our field data, the first to be obtained from an Alpine permafrost site where borehole temperatures are below -4°C, are promising for developing strategies of investigation of poorly known factors in steep bedrock permafrost such as the effect of snow cover and fracturing.

37

38

39

40

41

42

43

44

45

46

47

# 1 Introduction

The last few decades have seen an increase in rockfall activity from steep, high-altitude rock walls in the Mont Blanc Massif (Western European Alps) (Ravanel and Deline, 2010; Deline et al., 2012). Several studies of recent rock avalanches and rockfalls in mid-latitude alpine ranges have ascribed such increases to climate-related permafrost degradation (Deline, 2001; Gruber et al., 2004a; Huggel et al., 2005; Fischer et al., 2006; Huggel et al., 2008; Allen et al., 2009; Ravanel et al., 2010, 2012; Deline et al., 2011). Rockfall magnitude and frequency are thought to be linked to the timing and depth of permafrost degradation, which can range from a seasonal deepening of the active layer to long-term, deep-seated warming in response to a climate signal (Gruber and Haeberli, 2007). Local warming of cold permafrost may be

- induced by advection and the related erosion of cleft ice (Hasler et al., 2011b), which may lead to unexpected bedrock failures. As Krautblatter et al. (2011) noted, before being able to predict permafrost-related hazards, it is first necessary to develop a better understanding of the thermo-hydro-mechanical processes involved, which means collecting rock temperature
- 52 measurements and develop modeling strategies.
- 53 Measurement strategies and numerical experiments have been used to investigate the thermal 54 conditions and characteristics of near-vertical and virtually snow-free alpine rock walls that 55 are directly coupled with the atmosphere (Gruber et al., 2003; 2004b, Noetzli et al., 2007). 56 These studies have shown the domination of topography control on steep bedrock permafrost 57 distribution, with a typical surface temperature difference of 7-8°C between south and north 58 faces, the possible coexistence of warm and cold permafrost in a single rock mass and lateral 59 heat fluxes within the rock mass inducing near-vertical isotherms. Hasler et al. (2011a) suggested that, compared with snow-free, smooth rock faces, thin accumulations of snow on 60 micro-reliefs and cleft ventilation may both cause deviations of 1°C (shaded faces) to 3°C 61 62 (sun-exposed faces) compared with the smooth, snow-free rock wall model test case. The 63 thermal influence of snow on steep rock faces has been specifically addressed with numerical 64 experiments (Pogliotti, 2011), showing the high variability of its effect depending on 65 topography, depth and timing of the accumulation, but empirical evidences in such a context 66 are still scarce. These recent advances in the study of steep, alpine rock walls have helped to build bridges between what is known about the general characteristics of permafrost and 67 68 processes related to the microtopography and internal structure of the rock mass, which may 69 be significant in the short-term evolution and in permafrost distribution. However, a much 70 larger corpus of field observations and monitoring data for a variety of bedrock conditions is
- As part of our research into geomorphic activity in the Mont Blanc Massif, in 2005 we started a long-term permafrost-monitoring program at the Aiguille du Midi (AdM), that is presently the highest instrumented bedrock permafrost site in the European Alps (3842 m a.s.l). This monitoring program was designed to meet three scientific goals:
- 76 The monitoring program was designed to meet three scientific goals:

needed to develop, calibrate, and evaluate reliable models.

- 1. characterize the surface temperatures of high-alpine steep rock walls;
- 78 2. determine the thermal state of permafrost and analyze the variability of active-layer 79 and deep temperature;

- 3. collect temperature data under variable snow-cover and structural conditions useful for calibrating and validating high-resolution numerical experiments on permafrost thermal processes.
- 83 The present paper addresses goals (i) and (ii). It describes the monitoring program at the
- 84 AdM, presenting temperature data from nine surface mini-loggers and three 10metersdeep
- 85 boreholes. Due to the peak morphology of the AdM, the monitoring network is concentrated
- 86 in a very small area. The sensors are installed in order to investigate differing snow cover
- 87 conditions and bedrock structure. Such a network design allows to address the following
- 88 research questions:
- How much is the surface temperature variability due to topography in a so small area?
- 90 How much can be the thermal effect of snow cover on surface temperature in steep
- 91 rockwalls?
- 92 How much is the variability of active layer due to topography in steep rockwalls?
- What are the thermal effects of snow and fractures on sub-surface temperatures at the AdM?
- We analyze seasonal and annual patterns of surface temperature, active layer and permafrost
- 95 thermal regime from eight years of surface records and four years of borehole data discussing
- our results at the light of former studies and providing new empirical evidences of the poorly
- known effect of snow and fractures on permafrost in steep rock walls.

99

100

101

102

103

104

105

106

107

108

109

110

80

81

82

# 2 Study site

Located on the NW side of the Mont Blanc massif (Fig. 1), the summit of the AdM (45.88° N, 6.89°E) consists of three granite peaks (Piton Nord, Piton Central, and Piton Sud) and culminates at 3842 m a.s.l. The steep and partly glaciated north and west faces of the AdM tower more than 1000 m above the Glacier des Pélerins and Glacier des Bossons, while its south face rises just 250 m above the Glacier du Géant (i.e., the accumulation zone of the Mer de Glace). This part of the Mont Blanc Massif is formed by an inclusion-rich, porphyritic granite and is bounded by a wide shear zone. A main, N 40°E fault network intersected by a secondary network determines the distribution of the main granite spurs and gullies (Leloup et al., 2005). The highest parts of the peak tend to be steep, contain few large fractures, and, in places, are characterized by vertical foliation bands and small fissures. The lower parts are less steep and more fractured. In the present paper we use the abbreviation AdM to refer only

111 to the upper section of the Piton Central, between 3740 and 3842 m a.s.l. where most of the 112 instruments are installed. A tourist cable car runs from Chamonix to the Piton Nord. Galleries 113 and an elevator allow visitors to gain the viewing platform on top of the Piton Central, from 114 where there is a 360° panorama of the Mont Blanc Massif. 115 We chose the AdM as a monitoring site for the following scientific and logistical reasons: (i) 116 permafrost is extremely likely due to the AdM's high altitude and the presence of cold-based 117 hanging glaciers on its north face; (ii) the morphology of the peak, which offers a range of 118 aspects, slope angles, and fracture densities that are representative of many other rock walls in 119 the massif; (iii) the easy access by cable-car from Chamonix and the availability of services 120 (e.g., electricity) at the summit station. Monitoring equipment was installed as part of the 121 PERMAdataROC (2006–2008) and PermaNET (2008–2011) projects, funded by the 122 European Union and run jointly by EDYTEM Lab (France), ARPA VdA (Italy), and the 123 Universities of Zurich (Switzerland), Bonn, and Munich (Germany). As such it complements 124 other rock wall observation sites, for example, those within the Swiss Permafrost Monitoring 125 Network (PERMOS). 126 In complement to the monitoring equipment, weather stations from the ARPA VdA which 127 measured air temperature and relative humidity, incoming and outgoing shortwave and 128 longwave solar radiation, wind speed, and wind direction on the south and north faces worked 129 from 2006 to 2010. Electrical Resistivity Tomography (ERT) and Induced Polarization (IP) 130 are measured since 2008 with the Universities of Bonn and Munich. High-resolution (cm-131 scale) triangulated irregular networks (TIN) of rock walls and galleries of the AdM were 132 obtained from terrestrial laser scanning. Six crack-meters equipped with a wireless sensor 133 network were installed in July 2012 at major fractures of the Piton Central and Piton Nord to 134 complete existing studies of cleft dilatations and shearing movements in rock wall permafrost,

135

136

137

138

but will support our project.

to check the AdM stability and to test an early warning system. Finally, two GPR surveys

were performed along vertical transects since 2013. All these data are not used for this study

### 3 Data collection methods

139

140 3.1 **Rock temperature monitoring** 141 The present study uses rock surface temperatures at the top of the AdM (between 3815 and 142 3825 m a.s.l.; Fig. 2) that is monitored since 2005 using mini-loggers (GeoPrecision PT1000 143 sensors, accuracy ±0.1°C) and was installed by the University of Zurich and ARPA VdA. 144 Each face of the AdM has two loggers installed in snow free locations (Table 1). The south 145 face has an additional logger (S3) installed just above a small ledge on which snow 146 accumulates in winter, covering the logger. The loggers record the temperature every hour at 147 depths of 0.03, 0.30, and 0.55 m, in line with the method described by Gruber et al. (2003). 148 In September 2009, three boreholes were drilled in the lower section of the Piton Central, at 149 between 3738 and 3753 m a.s.l. 150 In order to minimize possible thermal disturbances, the boreholes were drilled several tens of 151 meters below the galleries running through the AdM. The possible disturbances in the Piton 152 Central are assumed to be related to air ventilation and heating from the local workers team 153 rooms especially, but because of the pluri-decametric vertical distance in between the 154 galleries and the boreholes, we assume that these last ones are not affected by the 155 anthropogenic disturbance. The exact location of each borehole was chosen according to the 156 aspect, fracturing, roughness, and angle of the rock wall (Fig. 2). Each borehole was drilled 157 perpendicular to the rock surface and to a depth of 11 meters. Borehole depths were 158 constrained by the drilling equipment and the funding available. The boreholes on the 159 northeast (BH\_E) and south (BH\_S) faces were drilled in fractured rock walls that slope at 65° and 55°, respectively. Even on rock walls at these angles, snow can accumulate on the 160 161 micro-reliefs in the face. The borehole on the northwest face (BH\_N) was drilled in a vertical, 162 unfractured wall. The only place that snow can accumulate on this wall is on small ledges 163 such as the one above which BH N was drilled. The boreholes were drilled between September 14<sup>th</sup> and September 27<sup>th</sup>, 2009 by a team of 164 165 five people (two mountain guides, plus three members of the EDYTEM Lab) who had to 166 contend with very variable weather and challenging logistics. For each borehole it was 167 necessary to: (i) install a safety line for the workers, (ii) set up a rope system to carry the 168 equipment from the galleries to the drill site, (iii) install a work platform for the three drillers, 169 (iv) anchor a base on which to fix a rack way, (v) drill the hole using a 380-V Weka 170 Diamond-Core DK 22 electric drill, (vi) insert into the hole a polyethylene PE100 tube (outer

diameter: 40 mm; inner diameter: 29 mm) sealed at its bottom, and (vii) remove the work platform. In addition to the difficult environment and harsh weather, the drilling work was complicated by the heterogeneity and hardness of the granite, which took a heavy toll on the equipment (11 diamond heads worn out or broken, a dozen steel tubes damaged, and a motor broken). At first we tried to drill 46-mm-diameter boreholes but we had to increase the diameter to 66 mm so we could use a more robust pipe string. Cooling required 1 to 3 m<sup>3</sup> of water per day, which was carried up from Chamonix in 1-m<sup>3</sup>-tanks via the cable car. Space between the drilling hole and the casing tube has not been filled.

The three boreholes were fitted with Stump 10-m-long thermistor chains, each with 15-nodes (YSI 44031 sensors, accuracy ±0.1°C) arranged along a 6-mm fiberglass rod. Following calibration at 0°C in an ice-water basin, the sensors were inserted in BH S and BH N in December 2009 and in BH E in April 2010 (Fig. 3). In order to prevent heat convection, each sensor was separated from the others on the chain by insulating foam. The boreholes were closed at the top, but the chains can be removed to check for thermistor drift. Rock temperatures at depths between 0.3 and 10 m are recorded every three hours (Table 1). Because BH\_S is shallower than 10 m, the thermistor chain protrudes from the rock surface by 36 cm. Temperature comparisons between BH S and BH N/BH E were carried out at the closest equivalent depths (e.g., temperatures at a depth of 2.64 m in BH\_S were compared with temperatures at a depth of 2.5 m in BH E and BH N).

190

191

198

201

171

172

173

174

175

176

177

178

179

180

181

182

183

184

185

186

187

188

189

#### 3.2 Air temperature and snow cover measurements

- 192 To support the analysis of rock temperature, we use air temperature that is monitored by 193 Météo France since 2007 at a station located 3 m above the top of the Piton Central (3845 m 194 a.s.l.) Data prior to 2007 (1989–2006) are very fragmented due to insufficient equipment 195 maintenance and are not used in this study in which we only use air temperature time series 196 (AT, Table 1).
- 197 In January 2012, two automatic cameras taking six pictures per day of the south and northeast borehole sites have been installed. In addition, five graduated stakes have been placed in the 199 surroundings of each borehole to evaluate the spatial variability of snow accumulation on 200 pictures. The visual analysis of pictures of winters 2012 and 2013 reveals a spatially homogeneous thick snow cover (>1m) lasting until late spring on BH\_S and a thin (<0.5 m) 202 spatially variable snow cover on the BH E due to the higher steepness and complex

geometry of the rock mass These observations are reported in Table 1. Snow accumulation over BH\_N and S3 is estimated from field observations. At BH\_N, snow accumulation is restricted to the relatively large ledge above which the borehole is drilled and the snow patch is over 1 m thick for most of the year. S3 is also frequently covered by > 0.5 m of snow accumulating during winter and spring on the small ledge above which the sensor is installed. But snow depth is more variable on S3 than on BH\_N because of the intense solar radiation that leads to more frequent melting.

210

211

212

213

214

215

216

217

218

219

220

221

222

223

224

225

226

227

228

229

230

231

232

203

204

205

206

207

208

209

# 4 Dataset preparation

The borehole time series are all continuous except for short periods for BH\_S, as this logger was removed from September 2012 to January 2013 and from October 2013 to January 2014 to prevent it being damaged by engineering work close to the borehole. Gaps in the 0.3 m temperature and AT time series were filled in so we could calculate seasonal and annual means (cf. Table 2). First, daily means from rock temperature time series were calculated for complete days of records. Then, short gaps (< 5 days) were filled by linear interpolation between the nearest available data points for the same depth; longer gaps (up to 1.5 month) were filled by replacing missing data with the average value for the 30 days before and 30 days after the gap (cf. Hasler et al., 2011a). To fill the longest gaps for E1, N1, S1, and W1 (from December 4<sup>th</sup>, 2007 to February 7<sup>th</sup>, 2008) we used a third approach that involved applying a linear regression equation, fitted using data from each pair of loggers (e.g., E2 and E1) and from the gap periods (i.e., December-February) for groups of years with complete records (2006–2007 and 2008–2009). Correlation coefficients for the equations ranged from 0.89 (S1 and S2) to 0.94 (E1 and E2). We tested this approach by simulating corresponding gap periods in the years with complete data and then filling these gaps using the regression equations. Differences between the annual means obtained using this method and the annual means calculated from the complete data set were in the range 0.01-0.15°C and can be considered negligible. Our calculations of seasonal means did not include data obtained using the 30-day average or linear regression methods. We did not fill gaps longer than 1.5 month per year because we felt that the resulting data would not be reliable enough to give realistic annual means.

# 5 Rock surface temperature

234

254

255

256

257

258

259

260

261

262

263

264

265

235 Smith and Riseborough (2002) defined Surface Offset (SO) as the difference between local 236 Mean Annual Air Temperature (MAAT) and Mean Annual Ground Surface Temperature 237 (MAGST). Surface offset is a parameter in the TTOP model (Temperature at the Top of 238 Permafrost, Smith and Riseborough, 1996), originally developed to define the functional 239 relation between air and ground temperatures in polar lowlands and later applied to high-240 latitude mountainous terrain (Juliussen and Humlum, 2007). SO can be used to quantify the 241 overall effect of ground cover and ground surface parameters on the surface energy balance. 242 We calculated both annual SOs (ASO), using annual means, and seasonal SOs (SSO) using 243 seasonal means of rock surface and air temperature of the season for winter (December to 244 February), spring (from March to May), summer (from June to August), and fall (from 245 September to November), using time series measured at depths of 0.3-m (boreholes and E2, 246 S2, W2, N2) and 0.1-m (E1, S1, W1, N1) - points we considered representative of surface conditions. We applied a standard lapse rate of 0.006°C.m<sup>-1</sup> on air temperature in order to 247 248 balance the elevation difference between the Météo France station and the sensors. Figure 4 249 shows ASOs for all the complete years (Fig. 4A), SSOs for snow-free sensors for the 250 available seasons (Fig. 4B), and SSOs for snow-covered sensors for the available seasons 251 (Fig. 4C). The SO description are then completed with the analysis of the daily temperature of 252 snow-covered sensors and air temperature trend (Fig. 5) to support the discussion on the snow 253 control on surface temperature.

# **5.1 Surface Offset patterns**

Spatially, maximum and minimum ASOs were 9.3°C, recorded at S1 in 2011, and 1.3°C, recorded at N1 in 2009 (Fig. 4A), which are typical values for the Alps (PERMOS, 2013). On the south face, the snow-covered sensors gave lower values than the snow-free sensors. For example, the ASOs for S3 were between 0.1°C (2010) and 1.4°C (2011) lower than the ASOs for S1. Conversely, on the north side, the snow-covered sensor gave higher ASOs than the snow-free sensors. At the seasonal scale, the maximum SSOs occurred in summer for the snow-free sensors (Fig. 4B), except for the sensors on the south face (S1 and S2), where the maximum SSOs occurred in spring, with values >10°C. The lowest SSOs were recorded in winter, and ranged from approximately 8°C on the south face to <1°C on the north face (N1 and N2). SSO patterns for the snow-covered sensors (Fig. 4C) were opposite to those for the snow-free sensors, except for BH\_E. At BH\_N and BH\_S, SSOs were largest in winter (4.1°C)

and 9.5°C, respectively) and lowest in summer. At S3, autumn SSO was the largest, and it was also relatively high for BH\_N and BH\_S. Unlike the other snow-covered sensors, SSOs at BH\_E remain coherent with insolation duration, similarly to snow free sensors.

Temporally, snow-covered and shaded sensors such as BH\_E and BH\_N show high interannual variability between 2011 and 2012 (+1.1°C), that is not visible at snow-free sensors, and at snow covered and south-facing sensors (only +0.3°C at S3). Conversely to the snow-covered sensors, the 2011-2012 ASO decreased at the snow-free sensors, with, for example, values of -1°C at S2 and -0.3°C at E1. The maximum and minimum ASOs for the different snow-free sensors did not occur in the same years. Even though both sensors of a similar aspect (e.g. N1 and N2) showed similar interannual changes, these changes were not consistent from one aspect to another, with, for example, the maximum ASOs at W1 and W2 in 2008, but in 2011 at S1 and S2.

### **5.2** Daily temperature of snow covered sensor

At the daily scale, temperature curves of the snow covered sensors are smoothed compared to air temperature oscillation during the cold period (Fig. 5). The S3 and BH\_S temperature curves were strongly smoothed from mid-November 2010 to January (BH\_S) or April 2011 (gap for S3), and from early December 2011 to mid-May 2012. Both sensors recorded a period of almost 0°C isothermal conditions from April to mid-May 2012. The temperature curve for BH\_N was strongly smoothed until the summer, with a similar 0°C isothermal period during three weeks in July 2011. Although the BH\_E temperature curve from late September to February-March was mostly smoother than the air temperature daily oscillations, both curves were more closely coupled than for the other sensors, as BH\_E oscillated in-synch with major changes in AT, such as the large drop in temperature in December 2012. The temperatures recorded at BH\_E were lower than those recorded at BH\_N during certain periods (September 2010 to March 2011, November 2011 to February 2012).

# 5.3 Snow cover and micro-meteorology influences

- Normally on steep, snow-free bedrock in high mountain, the MAGST is higher than MAAT.
- Such a difference is mainly due to direct solar radiation (Gruber et al. 2004b) and partly due
- 297 to reflected solar radiation from large, bright glacier surfaces below the measurement points

(PERMOS, 2013). In the European Alps, the ASO can be up to 10°C on south-facing rock walls. In Norway, maximum ASO values recorded on steep rock walls are only 3°C, as there is less direct solar radiation at the higher latitudes (Hipp et al., 2014). In New Zealand, thus at a similar latitude of the Alps, Allen et al. (2009) reported a maximum ASO value of 6.7°C. Such a lower value can be ascribed to a reduction of direct solar radiation due to the influence of the oceanic climate and related frequent cloud cover. In these studies most of the surface sensors have been installed in snow-free conditions with the purpose of testing energy balance models (Gruber et al., 2004b) or for statistical fitting (Allen et al., 2009, Boeckli et al., 2012). At the AdM patterns of snow-covered sensors are different from snow-free sensors, mainly due to the decoupling from the atmospheric conditions during the winter season and reduction of surface albedo. The differences in ASOs between snow covered and snow free sensors on similar aspect demonstrate that snow exerts a significant control on the annual energy balance. According to empirical and numerical studies (Hanson and Hoelzle, 2004; Luetschg et al., 2008), a snow thickness > 0.6-0.8 m insulates the rock surface from air temperature, but in steep rock walls, snow cover is usually thinner than this insulating threshold (Gruber and Haeberli, 2009). The differences between BH N and BH E in terms of ASOs and SSOs can be probably ascribed to variations of mean snow cover thickness (Table 1), and demonstrate that the insulating effect of snow can occur locally also in steep rock walls. On the north face, the higher ASOs at snow-covered sensors (BH N) compared to at snow-free sensors (N1 and N2) show that the thermo-insulation of snow significantly increases the MAGST. On the south face, the lower ASOs at snow covered sensors (BH\_S and S3) compared to snow free conditions (S1 and S2) indicates a lowering of MAGST due to snow. This cooling effect results from the combination of (i) a thin snow cover with negligible thermo-insulation, (ii) an increase of surface albedo, (iii) and melt energy consumption (Harris and Corte, 1992; Pogliotti, 2011). At the AdM, the latter two factors seems to be prevalent since the snow cover thickness on south face is proved to be often > 1 m during winter (sect 3.2) with appreciable smoothing of daily temperature oscillations (Fig. 5). This observation extents previous study on thin snow accumulations (Hasler et al. 2011a). The importance of this cooling effect on sunny faces is likely reinforced by the long lasting of the snow over the year at such elevation, as suggested by (i) the high autumn SSOs (early snow accumulation) for snow covered sensors, (ii) their low summer SSO, and (iii) by the nearly-isothermal conditions at 0°C occurring in late

298

299

300

301

302

303

304

305

306

307

308

309

310

311

312

313

314

315

316

317

318

319

320

321

322

323

324

325

326

327

328

summer (Fig. 5) and probably reflecting the zero-curtain effect (e.g. Hanson and Hoelzle, 2004; Gubler et al., 2011).

The inter-annual variability of ASO is not spatially homogeneous. Snow-covered and snowfree sensors exhibit different behavior, thereby complementing the PERMOS reports (2013), which showed differences in interannual variability between rock walls and gentle snowcovered terrain. The interannual variability of snow-free sensors is mainly related to differences in insolation due to clouds, and the differences within this interannual variability from on aspect to another can be interpreted as a difference in cloud formation from year-toyear. The difference in the spatial distribution of MAGST over a same rock peak due to the effect of convective cloud formations was already shown by energy balance models (Noetzli et al., 2007), but the evolution of these differences through time with the micrometeorological control was poorly explored. On shaded faces, the solar radiation control is largely reduced and snow may have more influence on the interannual changes. Consequently, the temperature at a snow-covered sensor can increase from one year to the next if the snow insulation from the atmospheric temperature increases meanwhile the temperature at a snow-free sensor may drop due to reduced insolation. In the case of sunexposed and snow covered sensor, such as S3, the balance between the warming and the cooling effects leads to smaller interannual ASO variability than at sensors in shadier locations mostly controlled by the warming effect of snow insulation. Thus, the snow influence on the surface temperature of high-elevated rock walls is a result of the combination between the topography, snow depth and micro-meteorology.

351

352

353

354

355

356

357

358

330

331

332

333

334

335

336

337

338

339

340

341

342

343

344

345

346

347

348

349

350

### 6 Borehole records

Four years of data from the three boreholes allowed us to describe the patterns of daily temperature (Fig. 6), mean annual Temperature-Depth (T(z)) profiles, and annual temperature envelopes (*i.e.*, the maximum and minimum daily temperatures at each depth in 2011; Fig. 7). We focused on the active layer and the permafrost thermal regime, paying special attention to thermal effects related to snow cover and bedrock structure which possible influence on the active layer and bedrock thermal regime is discussed in the light of present knowledge.

### 6.1 360 **Active layer** 361 Active Layer Thickness (ALT) varied with aspect, with means of ca. 3 m at BH\_E, 5.5 m at 362 BH\_S, and 2.2 m at BH\_N (Fig. 6). Interannual variability during the monitoring period was 363 ca. 0.7 m for each borehole (Table 3). The maximum ALT for each borehole occurred in 2012 for BH\_N (2.5 m deep), in 2013 for BH\_E (3.4 m deep), and in 2011 for BH\_S (5.9 m deep; 364 365 however, there are no relevant data for 2012). 366 The length of the thawing period, marked by continuous positive temperatures at the 367 uppermost thermistor, also varies according to aspect. It is longest at BH\_S, starting in June 368 (April in 2011), but with isolated thawing days already in March (e.g., in 2012). In general, 369 BH\_S surface refroze in October but total refreezing of the active layer did not occur until 370 December in 2010 and 2011. The 2011–2012 freezing period was particularly mild and short 371 (3–4 months) at BH S. This pattern was not as marked at BH E, which even recorded its 372 lowest surface temperature in 2011–2012. BH\_N had the longest freezing periods because 373 temperatures in the rock sub-surface remained positive only from June to October. In 2011, 374 thawing did not start until August. BH\_E had the most balanced thawing and freezing periods 375 (ca. 6 months each). 376 The timing of maximum ALT depended on aspect and year (Table 3). In 2010 and 2011, 377 maximum ALT occurred earliest at BH\_E, even though the active layer was thicker at BH\_E 378 than at BH N. In 2012 and 2013, BH N was the first site to reach maximum ALT. In 2010, 379 maximum ALT at BH S occurred very late, three months later than at BH E. Although the BH S active layer had mostly thawed by mid-July, thawing continued steadily until the end of 380

383

384

381

382

# **6.2** Thermal regime

lowering of the 0°C isotherm was more linear.

Annual Temperature-Depth T(z) profiles (Fig. 7A) revealed different thermal regimes. The AdM's Piton Central has both warm (ca. -1.5°C at BH\_S) and cold (ca. -4.5°C at BH\_N) permafrost (Table 3). Interannual changes were not similar in every borehole. In BH\_N and BH\_E the changes along the 2010-2013 period generally followed the changes in MAAT all along the T(z) profiles (Table 3), except for 2011 in BH\_N that is significantly warmer than other years from the surface to 2.5 m-depth and is colder than 2012 from 3 m-depth and than

October. Maximum ALT always occurred later at BH S than at the other boreholes, but the

2013 from 7 m-depth. In BH\_S, the mean annual T(z) profile of 2011 remarkably warms near the surface with positive temperatures to a depth of 1 m and is warmer than 2010 along the shallowest 6 m whereas it is slightly colder below.

The zero annual amplitude depth is >10 m for every borehole (Fig. 7B), which is consistent with other bedrock sites in the European Alps (PERMOS, 2007). In 2011, the largest amplitudes in daily temperature (peak to peak) at the surface (>20°C) and at 10 m depth (1.6°C) were at BH\_E, and the smallest surface (15.5°C) and 10-m (1.0°C) amplitudes were at BH\_N and BH\_S respectively. In line with the surface pattern, the minimum T(z) profile from the surface to 1.4 m deep was warmer at BH N than at the sunnier BH E (Fig. 7B).

The minimum and mean annual T(z) profiles for BH\_N contain two distinct sections separated by an inflection at ca. 2.5 m deep (Fig. 7A). This coincides with an 8–10 cm-wide cleft encountered at this depth during the drilling operation. The temperature gradient is negative (-0.39°C m<sup>-1</sup>) from the surface to the cleft, and then positive from the cleft to 10-m-deep (from 0.16°C m<sup>-1</sup> to nearly isothermal). The mean annual profiles for BH\_E are almost linear and have a temperature gradient of ca. -0.2°C m<sup>-1</sup>. Small inflections in the profiles (e.g., at 1.1 m, 2.5 m, and 7 m depth) occur every year. In the case of BH\_S, the upper parts of the annual T(z) profiles for 2010 and 2011 differ greatly, with an almost linear temperature gradient of -0.07°C m<sup>-1</sup> in 2010, and a much steeper overall temperature gradient of -2.26°C m<sup>-1</sup> in 2011.

# 6.3 Snow cover and bedrock discontinuity controls

- The coexistence of warm and cold permafrost and the opposite temperature gradients between BH\_S and BH\_N, that likely result from lateral heat fluxes, is in accordance with previous
- statements deriving from numerical simulations (Noetzli et al. 2007).
- In terms of permafrost thermal regime, the BH\_N shows deep temperatures colder than -4°C
- that is a value typical of high latitude monitoring sites such as in Svalbard (Noetzli et al.,
- 417 2014a) or the warmest boreholes of the continuous permafrost zone in Alaska (Romanovsky
- 418 et al., 2014).
- The spatial and temporal variability of ALT is consistent with values reported for Swiss
- boreholes in bedrock (PERMOS, 2013). For instance, thickness and timing of the ALT in
- 421 BH\_E are similar to those reported at the Matterhorn-Hörnligrat site (3295 m a.s.l, vertical
- borehole on a crest), with values ranging from 2.89 to 3.66 m between 2008 and 2010, and

423 maximum depth occurrence from early September to early October. In bedrock slopes, active 424 layer thickness changes seem strongly controlled by summer air temperature. During the hot 425 summer of 2003 for instance, the ALT at Schilthorn (2909 m a.s.l) has been deepened by 426 twice, from 4-5 m to > 8 m depht while on debris-covered slopes such as Les Gentianes 427 moraine or the Arolla scree slopes, located in the same area and at similar elevations, any 428 specific thickening has been observed (PERMOS, 2013). 429 The different patterns of ALT variability observed at the AdM between the three boreholes 430 (Table 3), suggest that the air temperature is not the only controlling factor. The thinning of 431 BH E active layer in 2011 in contrast with other two boreholes may be ascribed to the 432 cooling effect of a summer snow fall, but the cameras and snow probes were not installed yet (sect. 3.2) to check this hypothesis. However, a significant drop in daily SO at BH E occurred 433 just after three precipitation episodes (in August, the 26<sup>th</sup>, and in September, the 3<sup>rd</sup>-4<sup>th</sup> and 434 16<sup>th</sup>-19<sup>th</sup>), which supports this hypothesis but is hardly visible on a plot. These events 435 436 occurred just before BH\_N maximum ALT in 2011 (Table 3). Daily SO generally decreased 437 at BH\_S just after the precipitation events, and then, rapidly increased. The snow fall would 438 have rapidly melted and shortened its cooling effect compared to the more shaded BH\_E. 439 BH N rather showed a general increase of its daily SO, which possibly reflects a thermo-440 insulating effect. 441 The relatively mild and short 2011-2012 freezing period at BH\_S may result of snow 442 insulation, as is suggested by the subsequent period of isothermal conditions from the surface 443 to a depth of 3-m, which may reflect the zero-curtain effect (see sections 5.2 and 5.3). As 444 reported by Hoelzle et al., 1999, a thick long lasting snow cover reduces both the active layer 445 freezing by insulating from cold temperature and the active layer thawing by late snow 446 melting. Such an effect on the active layer freeze and thaw cycles is known from studies on 447 gentle morphologies and is poorly known in steep bedrock permafrost (Gruber et al. 2004a). 448 A clear effect of snow insulation is visible comparing temperature variations of BH\_E and 449 BH\_N (Fig. 5). In particular the winter surface temperature in BH\_N are always warmer and 450 smoothed than those in BH\_E (Fig. 5) and in depth (Fig. 7B), such a warming effect of snow 451 seems to propagate until 1.4 m. In terms of ALT, the tendency to thickening in BH\_E 452 compared to BH N and BH S (Table 3) may be explained by the effect of a long-lasting 453 snow cover on the latter two boreholes. 454 The interannual variability of ALT is usually greater on sun-exposed faces as they respond as 455 much to the change in air temperature as in solar radiation (Gruber et al. 2004a). However, BH S shows similar changes than the more shaded BH E and BH N. Field observations during drilling have revealed the presence of wet-detritic materials in the fractures of this face which suggests latent heat consumption interstitial water and/or ice during phase-change that may explain this incoherence. Moreover, the active layer of BH S shows late refreezing, especially in its deepest layers that can refreeze a few months after the surface (sect. 6.2, Fig. 6), which is also coherent with latent heat effects. This assumption is supported by previous studies explaining the delaying and dampening effect of latent heat consumption on the thermal response of bedrock permafrost (Kukkonen et Safanda, 2001; Wegmann et al. 1998, Noetzli et al. 2007). BH S patterns would demonstrate that this process may also be visible at short-time scale in steep rock walls. The cooling from 2010 to 2011 of its mean annual T(z) profile from 6 to 10-m-depth which is inconsistent with the MAAT change (Fig. 7, Table 3) also supports this assumption as this likely results of a dampened and delayed response. The probable control of latent heat in BH\_S is reinforced by its temperature range which allows for phase-change processes. The snow accumulation and melting on the south face constitute an obvious source of water supply to fill bedrock discontinuities. Such possible latent heat controls are not visible at BH\_E and BH\_N, which interannual changes are coherent with MAAT changes up to 10-m-depth, except for BH N in 2011 (Fig. 7A). The significant warming above the cold inflection is in coherence with MAAT change from 2010 to 2011, but the colder conditions below the inflection has no coherence with climatic signal. The fracture seems to act as a thermal cutoff between the surface layer and the deep bedrock. The sharp inflection of the profiles at the fracture depth, especially visible in the mean and minimum annual T(z) profile indicates that the fracture locally cools the rock. Mean annual temperature at 2.5-m-depth is even colder than the surface which, as said, is likely warmed by the snow cover. Such a cooling effect may result from air ventilation in the open fracture that has been shown as a important cooling factor of steep rock wall permafrost (Hasler et al. 2011a). Nevertheless, despite this dominant cooling effect, water percolation can occur along the fracture and heat advection could locally warm the rock (Hasler et al. 2011b), but no signal is detected in such sense on the temperature of BH\_N. The small inflections visible in BH E at several depths every year (sect. 6.2) are also possibly induced by bedrock discontinuities, but they have a negligible impact on the overall linear profile which indicates that heat conduction is the dominant heat transfer process (Williams and Smith, 1989). The fracture width is probably the critical factor controlling the magnitude of the perturbation. Thus, the AdM active layer and permafrost temperatures are controlled by different factors

456

457

458

459

460

461

462

463

464

465

466

467

468

469

470

471

472

473

474

475

476

477

478

479

480

481

482

483

484

485

486

487

interacting each other such as the snow cover and latent heat which delay and dampen shortterm responses to climate signal and cooling effect due to air ventilation within open fractures.

492

493

503

504

505

506

#### 7 Conclusion

- The high elevation, morphology and accessibility of AdM make it an exceptional site for investigating permafrost of steep rock walls. The available dataset include eight years of rock surface temperature and four years of deep temperatures. The monitoring network of AdM has been designed for investigating the thermal effect of topography, snow cover and fractures on permafrost. The analysis of this new dataset allows for confirmation of previous studies, some of them being empirically proved for the first time:
- 1. The thermal characteristics of the AdM's rock walls are typical of steep bedrock permafrost. The spatial variability of surface temperature, active layer thickness and timing, and the permafrost thermal regime are mainly controlled by topography.
  - 2. Deep temperature data confirm the characteristics of sub-surface thermal regime predicted by numerical experiments, in particular the coexistence within a single rock peak of warm and cold permafrost, which generates lateral heat fluxes from warm to cold faces.
- 3. Interannual changes of MAGST are not uniform at all aspects, even in snow free conditions. This may be ascribed to variable cloud formation from year-to-year.
- 4. Interannual change of snow-covered sensors may be opposite to snow free sensors as the snow can increase the MAGST due to higher thermo-insulation (more precipitations) meanwhile MAGST at snow free sensors can decrease because of reduced solar radiation and lower air temperature.
- 5. Surface temperature data confirm that a thin (not-insulating) snow cover is able to lower the MAGST because of a strong reduction of surface albedo.
- 515 6. Open fractures have a strong, localized cooling effect possibly resulting from air ventilation within the fracture.
- Observations from previous studies are extended and new characteristics are highlighted:
- 7. On south faces, a thick (insulating) snow cover may cool the MAGST because of a prevailing effect of increased surface albedo and latent heat consumption. On north faces, thermo-insulation can dominate and snow can warm MAGST similarly to gentle mountain slopes.

- 522 8. The interannual changes of MAGST in snow covered areas are greater on shaded 523 aspects than on sunny faces because the latter combines the controls of solar radiation and 524 snow.
- 9. The effects of snow cover on ALT in steep rock walls follow the same rules of gentle morphologies. In particular: (i) a thick (insulating) snow cover may reduce cooling during winter leading to a thickening of ALT; (ii) a long-lasting (early summer) snow cover may reduce summer warming leading to a thinning of ALT. Such a contrasting effects may coexist or not both in space (e.g. aspects) and time (e.g. season).
  - 10. Latent heat due to phase change processes of interstitial water in bedrock fractures can dampen active layer and permafrost interannual changes in steep bedrock.

533

534

535

536

537

538539

540

541

542

543

544

545

546

547

548

549

530

531

# 8. Further developments

- The AdM thermal characteristics illustrate the complexity of processes controlling the thermal regime of shallow layers in rock wall permafrost that currently challenges model development. Specific investigations addressing the snow control effect may be required to better understand the impact of thick snow accumulations and summer snow falls on ALT and permafrost changes which may contribute in the knowledge development on rock fall activities. The detailed analysis of the pictures showing the evolution of the south and northeast faces, of the snow probes and borehole records at the AdM, will support this project. Investigations on the latent heat consumption in compact bedrock may also be relevant to better understand ALT changes and timing of some snow-covered faces, as well as permafrost evolution over short-time scales. The BH\_N fracture constitutes an opportunity to investigate non-conductive heat transfers with adapted method such as a heat conduction scheme. Ground-penetrating radar measurements performed on the northwest face and crossing BH\_N borehole offer a clear image of the bedrock discontinuities and constitute additional data for heat flow model development that would integrate the bedrock structure. The combined use of crack-meters, air temperature and boreholes data is promising for developing the understanding of the thermal and mechanical factors in rock wall instabilities.
- The here presented data set has been used for statistical and numerical model evaluations designed for mapping the permafrost distribution in the Mont Blanc massif (Magnin et al., 2014) and for predicting the temperature field distribution and evolution over the next century at the AdM (Noetzli et al., 2014b). The statistical model will be used for determining the bedrock temperature and related permafrost thermal regime at the inventoried rock fall locations to analyze the relationship between bedrock temperature and failure.

Acknowledgements: We acknowledge S. Gruber, U. Morra di Cella, E. Cremonese and E. Malet for their participation in installation and data acquisition at the Aiguille du Midi, as well as the Compagnie des Guides of Chamonix for their help in the drilling operations, the Compagnie du Mont Blanc (especially E. Desvaux) for the access at the site, and Météo France for the air temperature data. We thank A. Hasler and anonymous reviewer for their useful comments and recommendations, and P. Henderson for improving the quality of the English language. This work is supported by the Region Rhône-Alpes (CIBLE program).

### 566 References

567

- Allen, S. K., Gruber, S., and Owens, I. F.: Exploring steep bedrock permafrost and its
- 569 relationship with recent slope failures in the Southern Alps of New Zealand, Permafrost
- 570 Periglac., 20, 345–356, doi:10.1002/ppp.658, 2009.

571

- 572 Boeckli, L., Brenning, A., Gruber, S., Noetzli, J. Permafrost distribution in the European
- 573 Alps: calculation and evaluation of an index map and summary statistics. The Cryosphere
- 574 Discuss., 6, 849–891, doi:10.5194/tcd-6-849-2012. 2012.

575

- 576 Cermak, V., Rybach, L. Thermal conductivity and specific heat of minerals and rocks. In
- 577 Landolt–Börnstein Zahlenwerte and Funktionen aus Naturwissenschaften und Technik, Neue
- 578 Serie, Physikalische Eigenschaften der Gesteine (V/1a), Angeneister G (ed.). Springer: Berlin;
- 579 305–343. 1982.

580

- Deline P.: Recent Brenva rock avalanches (Valley of Aosta): new chapter in an old story?
- 582 Supplementi di Geografia Fisica e Dinamica Quaternaria, 5, 55–63, 2001.

583

- Deline, P., Alberto, W., Broccolato, M., Hungr, O., Noetzli, J., Ravanel, L., and Tamburini,
- 585 A.: The December 2008 Crammont rock avalanche, Mont Blanc massif area, Italy, Nat.
- 586 Hazard Earth Sys., 11, 3307–3318, 2011.

587

- Deline, P., Gardent, M., Magnin F., and Ravanel, L.: The morphodynamics of the Mont Blanc
- massif in a changing cryosphere: a comprehensive review, Geogr. Ann. A, 94(2), 265–283,
- 590 2012.

591

- 592 Fischer, L., Kääb, A., Huggel, C., and Noetzli, J.: Geology, glacier changes, permafrost and
- related slope instabilities in a high-mountain rock wall: Monte Rosa east face, Italian Alps,
- 594 Nat. Hazard Earth Sys., 6, 761–772, 2006.

595

- Gruber, S., and Haeberli, W.: Permafrost in steep bedrock slopes and its temperature related
- 597 destabilization following climate change, J. Geophys. Res., 112, F02S13,
- 598 doi:10.1029/2006JF000547, 2007.

599

- Gruber S., Haeberli W.: Mountain permafrost. *In*: Margesin R. (Ed.). Permafrost soils.
- 601 Biology series, Springer, 16: 33-44, 2009.

602

- Gruber, S., Peter, M., Hoelzle, M. Woodhatch, I., and Haeberli. W.: Surface temperatures in
- steep alpine rock faces: a strategy for regional-scale measurement and modelling, In: L.
- 605 Arenson (Editor), 8th International Conference on Permafrost, Proceedings. Swets &
- 606 Zeitlinger, Lisse, Zürich, pp. 325-330, 2003.

- 608 Gruber, S., Hoelzle, M., and Haeberli, W.: Permafrost thaw and destabilization of Alpine rock
- 609 walls in the hot summer of 2003, Geophys. Res. Lett., 31, L13504,
- 610 doi:10.1029/2004GL0250051, 2004a.

- 612 Gruber, S., Hoelzle, M., and Haeberli, W.: Rock-wall temperatures in the Alps: modelling
- 613 their topographic distribution and regional differences, Permafrost Periglac., 15, 299–307,
- 614 doi: 10.1002/ppp.501, 2004b.

615

Gubler, S., Fiddes, J., Keller, M., Gruber, S.: Scale-dependent measurement and analysis of ground surface temperature variability in alpine terrain, The Cryosphere, 5, 431–443, 2011.

618

- Hanson, S. and Hoelzle, M. The thermal regime of the active layer at the Murtèl rock glacier
- 620 based on data from 2002. Permafrost Periglac., 15: 273–282. doi: 10.1002/ppp.499. 2004.

621

- Harris, S., and A. Corte (1992), Interactions and relations between mountain permafrost,
- 623 glaciers, snow and water, Permafrost Periglac., 3(2), 103–110.

624

- Hasler, A., Gruber, S., and Haeberli, W.: Temperature variability and offset in steep alpine
- 626 rock and ice faces, The Cryosphere, 5, 977–988, doi:10.5194/tc-5-977-2011, 2011a.

627

- 628 Hasler, A. Gruber, S. Font, M. Dubois, A. Advective heat transport in frozen rock clefts -
- 629 conceptual model, laboratory experiments and numerical simulation. Permafrost Periglac., 22,
- 630 378–349, doi: 10.1002/ppp.737, 2011b.

631

- Hipp, T., Etzelmüller, B. and Westermann, S. Permafrost in Alpine Rock Faces from
- 633 Jotunheimen and Hurrungane, Southern Norway. Permafrost Periglac., 25: 1–13.
- 634 doi: 10.1002/ppp.1799, 2014.

635

- Hoelzle, M., Wegmann, M. and Krummenacher, B.: Miniature temperature dataloggers for
- mapping and monitoring of permafrost in high mountain areas: first experience from the
- 638 Swiss Alps. Permafrost Periglac., 10: 113–124. doi: 10.1002/(SICI)1099-
- 639 1530(199904/06)10:2<113::AID-PPP317>3.0.CO;2-A, 1999.

640

- Huggel, C., Caplan-Auerbach, J., and Wessels, R.: Recent extreme avalanches triggered by
- climate change, EOS, Transactions American Geophysical Union, 89: 469–470, 2008.

643

- Huggel, C., Zgraggen-Oswald, S., Haeberli, W., Kääb, A., Polkvoj, A., Galushkin, I., and
- 645 Evans, S.G.: The 2002 rock/ice avalanche at Kolka/Karmadon, Russian Caucasus: assessment
- of extraordinary avalanche formation and mobility, and application of Quick- Bird satellite
- 647 imagery, Nat. Hazard Earth Sys., 5, 173–187, doi:10.5194/nhess-5-173-2005, 2005.

648

- Krautblatter, M., Huggel, C., Deline, P., and Hasler, A. Research Perspectives on Unstable
- 650 High-alpine Bedrock Permafrost: Measurement, Modelling and Process Understanding.
- 651 Permafrost Periglac., 23: 80–88, DOI: 10.1002/ppp.740 2011.

- Juliussen, H. and Humlum, O. Towards a TTOP ground temperature model for mountainous
- 654 terrain in central-eastern Norway. Permafrost Periglac., 18: 161–184. doi: 10.1002/ppp.586,
- 655 2007.

- Kukkonen, I. T., and J. Safanda. Numerical modelling of permafrost in bedrock in northern
- Fennoscandia during the Holocene, Global Planet. Change, 29, 259–273, 2001.

659

- Leloup, P. H., Arnaud, N., Sobel, E. R. and Lacassin, R.: Alpine thermal and structural evolution of the highest external crystalline massif: The Mont Blanc. Tectonics, 24, TC4002,
- doi: 10.1029/2004TC001676, 2005.

663

- Le Roy, M.: Reconstitution des fluctuations glaciaires holocènes dans les Alpes occidentales,
- Thèse de Doctorat de Géographie, Université de Savoie, Le Bourget du Lac, 344 pp, 2012.

666

- Luetschg, M., Lehning, M., and Haeberli, W.: A sensitivity study of factors influencing
- warm/thin permafrost in the Swiss Alps, J. Glaciol., 54, 696–704, 2008.

669

- Magnin, F., Brenning, A., Bodin, X., Deline, P., Ravanel, L. Manuscript submitted. Statistical
- modelling of rock wall permafrost distribution: application to the Mont Blanc massif.
- 672 Géomorphologie

673

- Noetzli, J., Gruber, S., Kohl, T., Salzmann, N., and Haeberli, W.: Three-dimensional
- distribution and evolution of permafrost temperatures in idealized high-mountain topography,
- 676 J. Geophys. Res-Earth, 112(F2), F02S13, doi:10.1029/2006JF000545, 2007.

677

- Noetzli, J., Christiansen, H. H., Guglielmin, M., Romanovsky, V. E., Shiklomanov, N. I.,
- Smith, A.L. and Zhao, L.: [Global climate] Permafrost thermal state [in "State of the Climate
- 680 in 2013"]. Bull. Amer. Meteor. Soc., **95** (7), S15–S16, 2014a.

681

- Noetzli, J., Ravanel L., and Deline P. in prep. Combining measurements and modelling to
- describe the permafrost conditions at the Aiguille du Midi (3842 m asl, Mont Blanc Massif).
- The Cryosphere.

685

- PERMOS: Permafrost in Switzerland 2002/2003 and 2003/2004, in: Vonder Mühll, D. (eds.),
- 687 Glaciological Report (Permafrost) No. 4/5 of the Cryospheric Commission of the Swiss
- Academy of Sciences, Zürich, 121 pp, 2007.

689

- 690 PERMOS: Permafrost in Switzerland 2008/2009 and 2009/2010, in: Noetzli, J. (eds.),
- 691 Glaciological Report (Permafrost) No. 10/11 of the Cryospheric Commission of the Swiss
- 692 Academy of Sciences, Zürich, 95 pp, 2013.

693

- 694 Pogliotti, P.: Influence of Snow Cover on MAGST over Complex Morphologies in Mountain
- 695 Permafrost Regions. PhD thesis, Turin, Italy, Università degli Studi di Torino. 79 pp. 2011.

- 697 Pogliotti, P., Cremonese, E., M. di Cella, U., Gruber, S., and Giardino M. Thermal diffusivity
- of Ninth International Conference variability in alpine permafrost rock walls, in Proceedings of Ninth International Conference
- on Permafrost, Fairbanks, Institute of Northern Engineering, University of Alaska, vol. 2, pp.
- 700 1427–1432, 2008.

Ravanel, L. and Deline P.: Climate influence on rockfalls in high-Alpine steep rock walls: the north side of the Aiguilles de Chamonix (Mont Blanc massif) since the end of the 'Little Ice Age', The Holocene, 21, 357–365, doi: 10.1177/0959683610374887, 2010.

705

Ravanel, L., Allignol, F., Deline, P., Gruber, S., and Ravello, M.: Rock falls in the Mont Blanc Massif in 2007 and 2008, Landslides, 7, 493–501, 2010.

708

Ravanel, L., Deline, P., Lambiel, C., and Vincent C.: Intability of a high Alpine rock ridge: the lower Arête des Cosmiques, Mont Blanc massif, France, Geogr. Ann. A, 95, 51–66, doi: 10.1111/geoa.12000, 2012.

712

Romanovsky, V. E., Smith, S. L., Christiansen, H. H., Shiklomanov, N. I., Streletskiy, G. A., Drozdov, D. S., Malkova, G. V., Oberman, N. G., Kholodov, A. L., Marchenko, S. S.: [Global climate] Terrestrial permafrost [in "State of the Climate in 2013"]. *Bull. Amer. Meteor. Soc.*, 95 (7), S139–S141, 2014.

717 718

719 Smith, M. W. and Riseborough, D. W. Permafrost monitoring and detection of climate 720 change. Permafrost Periglac., 7: 301–309. doi: 10.1002/(SICI)1099-721 1530(199610)7:4<301::AID-PPP231>3.0.CO;2-R, 1996.

722

Smith, M. W. and Riseborough, D. W. Climate and the limits of permafrost: a zonal analysis. Permafrost Periglac., 13: 1–15. doi: 10.1002/ppp.410, 2002.

725

Williams, P. J. and Smith, M. W.: The frozen earth, 1 ed., Studies in polar research, Cambridge University Press, Cambridge, 306 pp., 1989.

728 Tables

Site Code	Elevation [m a.s.l]	Aspect [°]	Slope [°]	Sensor depths [m]	Estimated snow accumulation [m]	
BH_S	3753	135	55	0.14, 0.34, 0.74, 1.04, 1.34, 1.64, 2.14, 2.64, 3.64, 4.64, 6.64, 8.64, 9.64	> 0.8	
BH_N	3738	345	90	0.3, 0.5, 0.7, 0.9, 1.1, 1.4, 1.7, 2, 2.5, 3, 4, 5, 7, 9, 10	> 1.0	
BH_E	3745	50	65	0.3, 0.5, 0.7, 0.9, 1.1, 1.4, 1.7, 2, 2.5, 3, 4, 5, 7, 9, 10	< 0.6	
$\mathbf{W1}$	3825	270	80	0.1	0	
S1	3820	140	74	0.1	0	
N1	3820	354	84	0.1	0	
<b>E</b> 1	3823	124	60	0.1	0	
N2	3820	334	80	0.03, 0.1, 0.3, 0.55	0	
<b>E2</b>	3820	118	60	0.03, 0.1, 0.3, 0.55	0	
<b>S2</b>	3815	160	85	0.03, 0.1, 0.3, 0.55	0	
W2	3825	270	85	0.03, 0.1, 0.3, 0.55	0	
<b>S3</b>	3820	158	70	0.03, 0.1, 0.3, 0.55	0.5 to 1.0	
AT	3845	0	0		0	

<sup>730</sup> **Table 1**. Instrument positions.

BH: borehole thermistor chains, x1 and x2: rock surface temperature loggers, AT: air temperature. Estimated snow accumulation: from automatic cameras and probes for BH\_S and BH\_E (winter 2011 and 2012), from field observation for S3 and BH\_N.

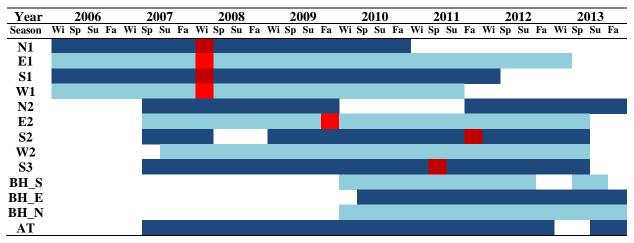


**Table 2.** Data availability after gap filling.

**Wi**: December, January, February; **Sp**: March, April, May; **Su**: June, July, August; **Fa**: 737 September, October, November.

Red sections indicate where gaps <1.5 month per year have been filled in order to calculate annual means but seasonal means were not calculated for the seasons in question. The time series interrupted with white gap areas indicate that annual mean is not computed for the concerned year.

	вн_е				BH_S			BH_N		MAAT
Year	ALT [m]	Max. ALT [dd.mm]	MART <sub>10m</sub> [°C]	ALT [m]	Max. ALT [dd.mm]	MART <sub>10m</sub> [°C]	ALT [m]	Max. ALT [dd.mm]	MART <sub>10m</sub> [°C]	
2010	3.1	27.07	-	5.2	23.10	-1.4	1.8	28.08	-4.7	-9
2011	2.7	30.08	-3.8	5.9	22.10	-1.5	2.3	18.09	-4.6	-6.7
2012	3.3	26.08	-3.6	-	-	-	2.5	26.08	-4.3	-7.7
2013	3.4	08.09	-3.6	5.8	30.09	_	2.2	25.08	-4.5	-

<sup>742</sup> **Table 3.** Borehole and air temperature records.

<sup>743</sup> ALT: Active Layer Thickness

<sup>744</sup> MART<sub>10m</sub>: Mean Annual Rock Temperature at 10 m deep

- 745 Figure captions
- 746 **Figure 1.** Location of the Mont Blanc Massif and the Aiguille du Midi (red triangle)
- 747 (modified from Le Roy, 2012).

- 749 **Figure 2**. The Aiguille du Midi with camera, RST, and BH logger locations.
- 750 *Pictures: S. Gruber (top left and right, bottom left); P. Deline (bottom right).*

751

- 752 **Figure 3.** Borehole positions and components.
- 753 Left: Horizontal cross-section through the AdM's Piton Central. Borehole positions are
- marked in red.
- Right: 10-m-long, 15-node thermistor chain installed in the boreholes.

756

- 757 **Figure 4.** Annual and Seasonal Surface Offsets calculated from sensors at 0.3 m deep.
- ASOs are shown for all the available years. SSOs are the mean values for the available
- seasons for each logger listed in Table 2.

760

- 761 **Figure 5.** Daily temperature records at 0.3 m deep for snow-covered sensors for the 2010-
- 762 2011 and 2011-2012 hydrological years.

763

- Figure 6. Daily temperature records in the AdM boreholes from December 2009 to January
- 765 2014.

766

Figure 7. Mean T(z) profiles (A) and 2011 temperature envelopes (B) of the AdM boreholes.